ACS OMEGA

http://pubs.acs.org/journal/acsodf

Article

Experimental Research on the Combustion Characteristics of Transformer Oil Jet Fires in Oil-Filled Equipment under Heat

Ruibang Sun, Juncai Wang, Xing Yang, and Peng Chen*

Cite This: *ACS Omega* 2021, 6, 31843−31853

Read Online

ACCESS | Metrics & More | Article Recommendations

ABSTRACT: Under the action of heat, the jet fire of oil-filled equipment in substations produces intense heat radiation and flame impact, causing serious harm to the personnel and equipment. Therefore, this paper has carried out a series of oil-filled equipment transformer oil jet fire experiments with different nozzle diameters to study the characteristics of transformer oil jet flame combustion. The experiment measured the mass loss rate, axial centerline temperature of the fire plume, and radiant heat flux and processed the flame visualization image. The results show that the combustion process of the transformer oil jet fire can be divided into three stages. The functional relationship between the flame height and mass flow and the functional relationship between the flame temperature and axial height are derived. A prediction model of the radiant heat flux of the transformer oil jet fire for the oil-filled equipment of the substation was established. The research results are of great significance for improving the fire protection design of substations and improving fire management and control capabilities.

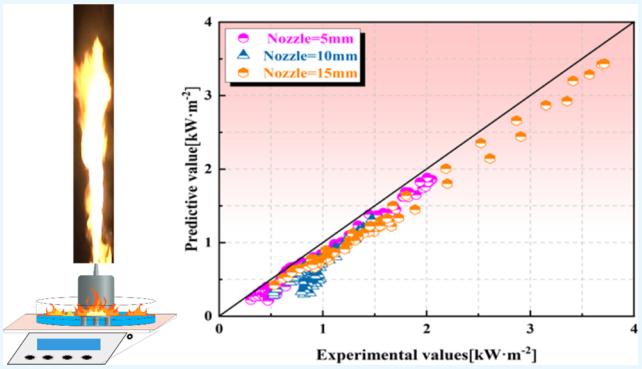

1. INTRODUCTION

As global climate warming becomes more and more significant, mankind continues to improve energy usage patterns. In this context, electric energy as a clean and efficient energy source has been widely used all over the world.[1−4] Substations play an important role in power transmission, so the development of the power industry is inseparable from the commissioning of a large number of substations. However, the safety issues of substations have always attracted the attention of scientific researchers. Due to the large amount of oil-filled equipment stored in the transformer substations, when the oil-filled equipment has an arc short circuit and other faults, it will cause the formation of a heat source outside of the oil-filled equipment and generate a transformer oil jet fire. Transformer oil jet flames pose serious safety threats to power equipment and workers due to their strong near-field heat radiation and long-distance flame impact.[5−9] Moreover, about 50% of jet fire accidents will induce a domino effect, which will lead to more serious accidents.[10] Therefore, it is necessary to study the combustion characteristics of transformer oil jet fires to provide theoretical help for substation fire prevention and control.

The combustion characteristics such as flame height,[11−19] flame temperature,[20−29] and radiant heat flux[30−43] in the process of jet fire combustion have received extensive attention from scholars. The height of the flame reflects the intensity of the combustion.[19] For this reason, scholars have carried out a lot of research on the relationship between flame height and fuel mass flow. Imamura[11] established the correlation between flame height and mass flow through hydrogen jet fire experiments. Mogi[12] carried out a series of experiments on liquefied dimethyl ether jet fire and got the prediction function of flame height. Zhang[13] determined the functional relationship between flame height and mass flow based on the *liquefied natural gas* jet fire experiment. In order to establish a jet fire height prediction model, Palacios[14] carried out the jet fire experiment of 11 different medium hydrocarbon fuels and established the prediction model of jet flame height. The flame temperature reveals the intensity of the combustion reaction.[22] The study of axial flame temperature is helpful for understanding the energy distribution of jet flames. The current research on flame temperature is mainly based on the three-zone theory of classical temperature distribution proposed by McCaffrey.[21] However, the research object of McCaffrey's three-zone theory is not suitable for jet fires with initial momentum. Zukoski[23] further improved the research object

Received: August 20, 2021
Accepted: November 5, 2021
Published: November 16, 2021

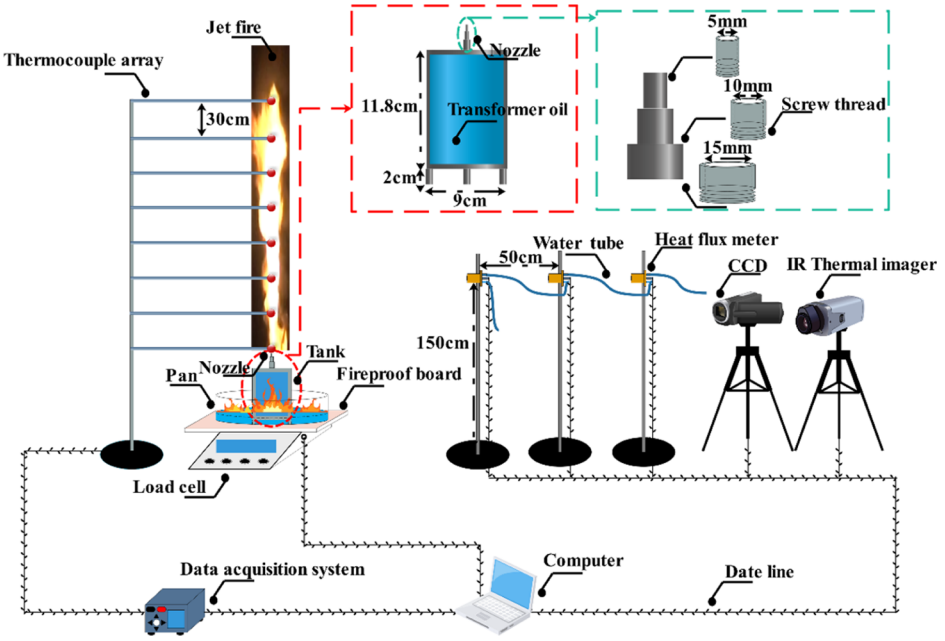

Figure 1. Schematic of the experimental system.

based on the three-zone theory and initially established a jet fire plume temperature prediction model. In order to further determine the relationship between the axial flame temperature and the axial distance, Gomez-Mares[29] carried out a series of commercial propane vertical jet fire experiments and obtained a quadratic polynomial to the axial centerline temperature and axial height of the fire plume. Flame radiant heat flux is one of the key parameters for evaluating fire hazards.[30] Jet fire has been widely studied by scholars because of its high radiant heat flux.[31] Research on radiant heat flux mainly focuses on two aspects: radiation fraction and radiation model. Zhou[33] clarified the key parameters that control the jet fire radiation fraction and established the correlation between the Froude number and the radiation fraction. Hu[37] conducted a series of jet fire experiments under different pressure environments and obtained the relationship between the radiation fraction and Reynolds number. Kang[42] uses the point source model and the multi-point source model to calculate the radiation fraction of the dimethyl ether jet fire. Palacios[34] evaluated the radiant heat flux of a series of outdoor jet fire experiments to the surrounding environment based on the solid flame model. At the same time, Gomez-Mares[41] studied the radiation intensity of propane jet fires based on the solid flame model. Hankinson[40] proposed a new radiation model based on hydrogen and methane/hydrogen jet fire experiments, namely, the multi-point source radiation model. Since then, Zhou[38,43] has further expanded the type of the radiation model, namely, the line source model, and he used propane jet fire experiments to compare the differences between the four radiation models.

It can be seen that scholars have conducted extensive research on the combustion characteristics of jet fires and have achieved remarkable results. However, the combustion characteristics of transformer oil jet fires are still unclear. It is worth noting that because the fuel medium of the transformer oil jet fire is a gas−liquid two-phase flow, the combustion characteristics of the common jet fire are significantly different.[41] When the fuel medium is a gas-phase flow, the fuel combustion efficiency is high due to the sufficient mixing of air and fuel. The color of the flame is almost transparent. The heat generated by combustion is mainly transferred to the outside world in the form of convection. However, when the fuel medium is a gas−liquid two-phase flow, the combustion situation is significantly different. Because the gas−liquid two-phase flow seriously affects the mixing degree of fuel and air, the combustion efficiency is low. Inefficient combustion is conducive to the production of carbon black particles, causing the color of the flame to appear yellow or even white. At the same time, the generated carbon black particles significantly enhance the radiant heat flux from the flame; the radiant heat flux emitted by the gas−liquid two-phase jet flame is higher than that of the gas-phase jet flame. In addition, the fuel mass flow rate increases due to the presence of liquid droplets, which promotes a significant increase in flame height. Therefore, the research on the combustion characteristics of transformer oil jet fires is more in line with the actual scene of substation fires.

This paper carried out a series of transformer oil jet fire experiments to study its combustion characteristics. To this end, three different-diameter nozzles were used in the experiment. First, the combustion process is divided by the mass loss rate, and the correlation between flame height and mass flow is obtained by processing the flame image. Then, combined with the empirical formula, the functional relationship between the axial flame temperature and the axial height is determined. Finally, based on the solid flame model, a prediction model of the radiant heat flux of the transformer oil jet fire was established. The research results have important theoretical value for the prevention of jet fire accidents in substations.

2EXPERIMENTAL SETUP

2.1Experimental System. All experiments were completed in a tunnel. During the experiment, the tunnel doors and windows (not sealed) were closed down to ensure that the flame burns in a still air environment. The schematic of the experimental system is shown in Figure 1.

https://doi.org/10.1021/acsomega.1c04551
ACS Omega 2021, 6, 31843−31853

The experimental system includes a fuel supply system and a data acquisition system. The fuel supply system consists of an oil storage tank, an oil pool, and KI25X transformer oil. The data acquisition system includes a temperature acquisition system, image acquisition system, quality acquisition system, radiant heat flux acquisition system, and data acquisition instrument. The oil storage tank in the fuel supply system is a cylindrical stainless-steel tank with a nozzle installed in the center of the top. The bottom is welded with three cylindrical brackets to form a vertical jet fire. The detailed parameters of the oil storage tank are shown in Table 1. The oil storage tank is placed in the center of the oil pool with a diameter of 30 cm and a side wall of 10 cm height. The fuel used in the experiment is KI25X transformer oil, and the specific physical parameters are shown in Table 1.

Table 1. Storage Tank Parameters and Properties of the KI25X Transformer Oil

parameters	value	properties	value
tank height (cm)	11.8	density (kg m^{-3})	883
tank diameter (cm)	9	flash point (°C)	155
tank wall thickness (cm)	0.5	heat conductivity (W m^{-1} K^{-1})	0.128
bracket height (cm)	2	heat capacity (J kg^{-1} K^{-1})	1960
bracket diameter (cm)	1.5	effective heat of combustion (MJ kg^{-1})	40

The temperature acquisition system consists of eight thermocouples. The spatial position of the thermocouple is shown in Figure 1, the bottom thermocouple is located 0 m above the nozzle (i.e., .at the nozzle), and the remaining thermocouples are arranged vertically and evenly upward along the centerline of the fire plume axis at 30 cm intervals to characterize transformer oil and axial centerline temperature of the jet fire plume. The temperature measurement end of the thermocouple is placed at the center line of the fire plume axis, and the other end is connected with the data line to convert the measured temperature data from an analogue signal to a digital signal and transmit it to the data acquisition instrument. The image acquisition system consists of a charge-coupled device (CCD) and an infrared (IR) thermal imager composition. The CCD is utilized to record the visual flame image. An IR thermal imager is used to record the real physical geometry. The two cameras are placed at the same position (the horizontal distance from the nozzle is 6 m, and the vertical distance from the ground is 1.5 m), and they are both placed perpendicular to the flame to record the geometric image of the flame. As the experimental background needs to maintain a dark environment, all experiments are carried out at night to effectively record the flame geometry image and reduce image noise. In order to obtain the height of the flame of the transformer oil jet, the flame image needs to be processed. First, the occurrence and development video of jet fire was intercepted from the video according to each working condition. Then, the intercepted video is decompressed into frames, and the color images are sequentially converted into grayscale images. Finally, based on the OTSU[44] methods, the image brightness threshold is dynamically determined, the gray image is converted into a binary image, and the characteristic parameters of the flame in the visualized image are obtained. The mass acquisition system consists of a load cell. The mass acquisition system can record the instantaneous mass loss rate of fuel in the fuel supply system to obtain the heat release rate during the combustion process. The radiant heat flux collection system consists of three water-cooled wide-angle heat flux meters. The three heat flow meters are kept at a vertical distance of 1.5 m from the ground. The receiving surface of one heat flux meter is at a horizontal distance of 1 m from the flame, and the remaining heat flux meters are placed in increments of 0.5 m in the radial direction. The receiving surface of the heat flux meter is kept perpendicular to the flame direction. The radiation signal received by the heat flux meter probe is converted into a voltage signal and transmitted to the data acquisition instrument. The maximum temperature of cooling water should not exceed 80 °C, and the flow rate should be 6 L/min. The data acquisition system consists of a data acquisition instrument and a computer. The experimental equipment configuration is shown in Table 2.

Table 2. Experimental Equipment Configuration

equipment	configuration	
K-type thermocouple	diameter: 1 mm	accuracy is less than 1 °C or 3%
SONY NEX-FS700 CCD	pixel: 1280 × 720	frame rate: 25 fps
DALI TECHNOLOGY DL700	pixel: 640 × 480	frame rate: 25 fps
IR thermal imager	precision: ±2 °C	maximum detection of a black body temperature of 1200 °C
AND GP-61ks load cell	precision: ±0.1 g	range: 0−60 kg
water-cooled wide-angle heat flow meter	diameter of sensitive area: 11 mm	top depth: 0.5 mm
	maximum range: 50 kW/m^2	
HIOKI LR840-21 data collector	acquisition frequency: 100 Hz	
DELL computer		

2.2Experimental Conditions. In this study, three different-diameter nozzles (5, 10, and 15 mm) were used as variables to carry out a series of transformer oil jet fire combustion experiments to study the characteristics of transformer oil jet fire combustion. All experimental conditions are shown in Table 3. In order to ensure the repeatability of the experiment, at least three experiments are carried out under each experimental condition, and the average value of the three sets of data is used as the experimental result. The weather station measured the ambient temperature, ambient pressure, relative humidity, wind speed, wind direction, and rainfall. The specific test conditions are shown in Table 4.

Table 3. Summary of Experimental Conditions

exp. id	nozzle diameter (mm)	liquid level (%)	pool diameter (cm)
1	5	100	30
2	5	100	30
3	5	100	30
4	10	100	30
5	10	100	30
6	10	100	30
7	15	100	30
8	15	100	30
9	15	100	30

https://doi.org/10.1021/acsomega.1c04551
ACS Omega 2021, 6, 31843−31853

Table 4. Test Conditions

properties	value
air temperature (°C)	25 ± 3
relative humidity (%)	70 ± 10
wind speed (m s^{-1})	0
wind direction	
rain (mm)	0
air pressure (kPa)	101 ± 5

2.3. Experimental Steps. The experimental steps of oil jet fire combustion of transformer oil-filled equipment in the substation are as follows:

(i)Check each system before the start of the experiment to ensure effective work.

(ii) After checking the various systems, open the water tube of the heat flux meter in advance to ensure that the heat flux meter conducts the experiment safely and effectively. First, inject 100%-liquid level transformer oil into the oil storage tank and inject transformer oil with a thickness of 3 cm into the oil pool. At the same time, turn on the electronic balance to record the fuel quality in the oil storage tank and the oil pool. Then, use a graduated cylinder to measure 10 mL of *n*-heptane, and add it to the surface of the oil pool. Finally, an electronic igniter is used to ignite the fuel supply system and start the data acquisition system. In addition, it is necessary to pay attention to adding a fireproof board between the oil tank and the automated balance to prevent the electronic balance from being damaged during the experiment.

(iii) After the experiment, close the data acquisition system, and save the collected data to the computer.

3. RESULTS AND DISCUSSION

3.1Combustion Behavior. The instantaneous mass loss rate curves of the three different-diameter nozzles are shown in Figure 2. It can be observed that the instantaneous mass loss rates of the three nozzle diameters have similar changing trends.

The jet fire combustion process of the oil-filled equipment with three different-diameter nozzles is shown in Figure 3a. The infrared image of the combustion process of oil-filled equipment with a nozzle diameter of 10 mm is shown in Figure 3b. Combining Figures 2 and 3, the jet fire combustion process of the oil-filled equipment in the substation is divided into three stages: i—growth stage; ii—decay stage; and iii—extinction stage.

(i) Growth stage (stage i): It can be seen from Figure 3 that after the external oil pool is ignited, the flame gradually spreads to the entire surface of the oil pool to heat the oil storage tank. Under the action of the external heat source, the nozzle of the top of the oil storage tank starts to spray out the jet fire flame, and the jet fire burns into the growth stage. The mass loss rate develops steadily and then rapidly increases to the peak. The jet fire appears at the corresponding inflection point (Figure 2). The height of the jet fire flame increased rapidly to the peak (Figure 3). At this stage, the degree of combustion of the jet fire gradually strengthens. The flame image is clear and bright with black smoke, and the radiant heat flux to the surrounding area is significantly enhanced.

(ii) Decay stage (stage ii): In this stage, a large amount of fuel is sprayed from the nozzle to participate in the combustion reaction. The maximum flame height is maintained for a short period of time and then begins to shrink downward. The mass loss rate decreases from the peak. The decrease in the mass loss rate can be attributed to the consumption and entrainment of a large amount of fuel. At this stage, the degree of jet fire combustion changes from strong to weak. Soot particles are produced during the combustion process and begin to accumulate on the top of the tunnel. The flame geometry is clearly visible, and the radiant heat flux to the surroundings gradually changes from strong to weak.

(iii) Extinction stage (stage iii): The flame attenuation trend is gentle. The flame tip slowly shrinks toward the nozzle until the flame disappears (Figure 3). The mass loss rate slowly decreases until it develops steadily again, and the jet fire is extinguished at the corresponding inflection point (Figure 2). At this stage, the height of the jet fire flame continues to decrease until the flame disappears. A large number of carbon black particles are generated by combustion and migrate from the top space of the tunnel to the surroundings, and the radiant heat flux from the flame to the surroundings gradually weakens to a stable level. After that, the external heat source keeps burning until it goes out.

3.2Flame Height. Combined with the research of domestic and foreign scholars,[45] this paper defines the geometric characteristics of the flame as follows (Figure 4):

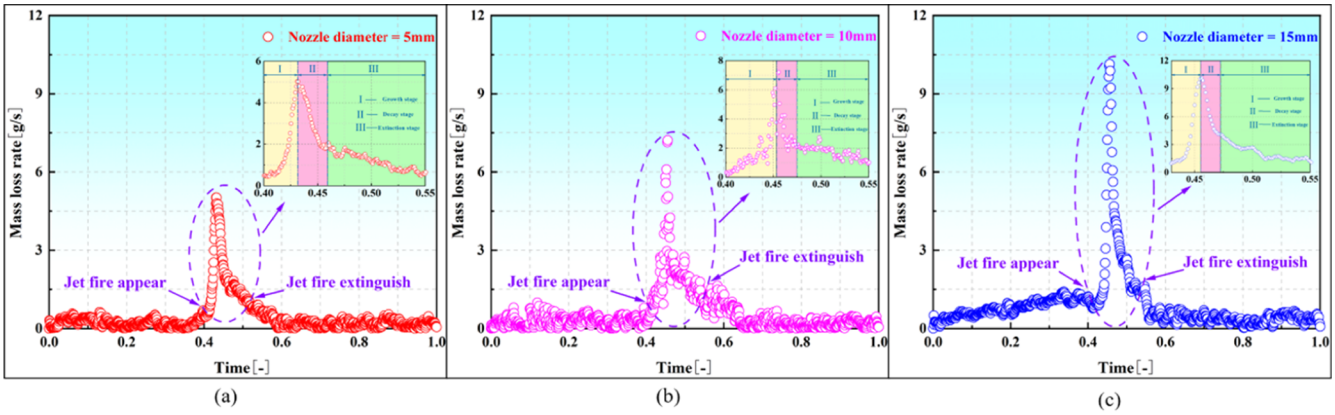

Figure 2. (a) Mass loss rate for a nozzle diameter of 5 mm. (b) Mass loss rate for a nozzle diameter of 10 mm. (c) Mass loss rate for a nozzle diameter of 15 mm. (Time [-] = T_{real}/T_{total}).

https://doi.org/10.1021/acsomega.1c04551
ACS Omega 2021, 6, 31843−31853

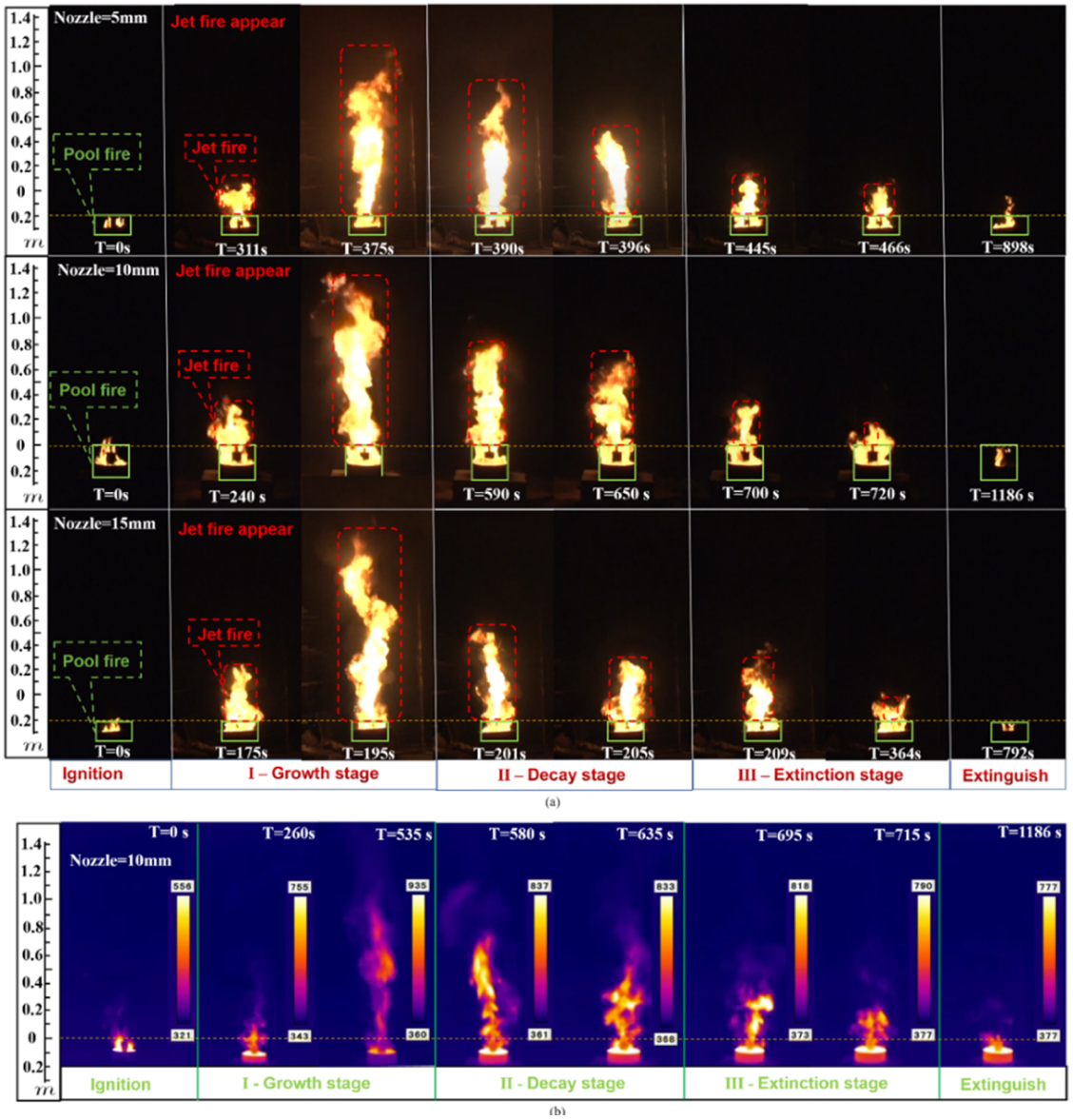

Figure 3. (a) CCD images of the combustion process of jet fire with three different-diameter nozzles. (b) IR images of the jet fire combustion process with a nozzle diameter of 10 mm.

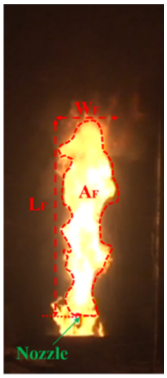

Figure 4. Flame geometry features of jet fires.

(i) flame height, L_F, the distance from the nozzle to the flame tip, (ii) flame width, W_F, the average width occupied by the flame transversely, and (iii) flame area, A_F, isothermal contour or visual flame surface.

Through visual image processing, the jet flame height curve of three different-diameter nozzles can be obtained (Figure 5). It can be seen from Figure 5 that first, the height of the jet fire flame increases, then remains stable for a short time, and finally decreases slowly. Jet flame height of different-diameter nozzles has a similar development trend. As the nozzle diameter increases, the peak jet flame height increases. In addition, there are significant differences in the peak flame height between a small nozzle diameter and large nozzle diameter. This difference can be attributed to the change in mass flow at the nozzle, since the mass flow rate at the nozzle increases significantly with the increase in diameter. Furthermore, the flame height can be increased with the following three aspects: the degree of mixing of fuel and oxygen; the combustion chemical reaction rate; and the efficiency of entraining oxygen.

The general correlation formula of transformer oil jet fire flame height was obtained with different-diameter nozzles. Based on the research of Palacios,[14] this paper uses experimental data to obtain the correlation between the

https://doi.org/10.1021/acsomega.1c04551
ACS Omega 2021, 6, 31843−31853

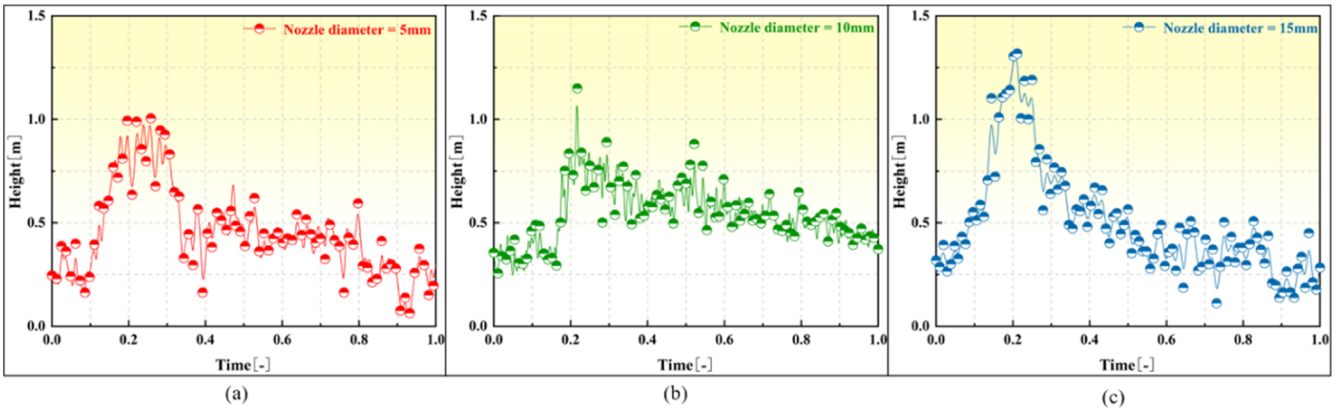

Figure 5. (a) Flame height evolution curves for a nozzle diameter of 5 mm. (b) Flame height evolution curves for a nozzle diameter of 10 mm. (c) Flame height evolution curves for a nozzle diameter of 15 mm.

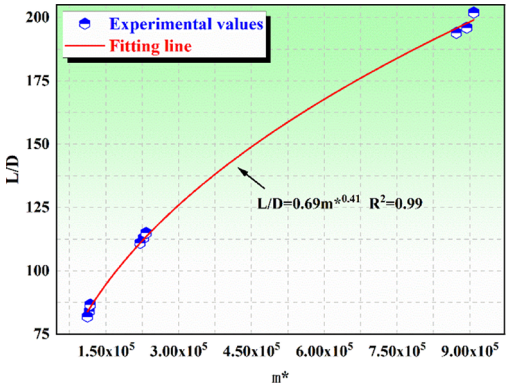

Figure 6. Fitting relationship between the dimensionless height and dimensionless mass flow.

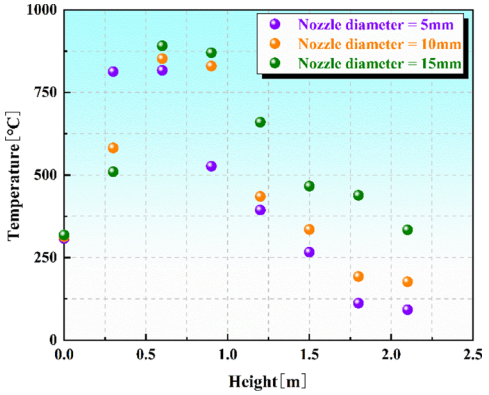

Figure 7. Axial temperature distribution of the fire plume of three different-diameter nozzles.

dimensionless flame height and the dimensionless mass flow rate (Figure 6). The experimental data in the figure better converge to the fitting curve.

$$m^* = \frac{\dot{m}}{\rho_\infty \sqrt{gD}} \tag{1}$$

where $\dot{m}$ is the mass flow rate per unit area (kg s^{-1} m^{-2}), ρ_∞ is the ambient density (g cm^{-3}), g is the gravitational acceleration (m s^{-2}), and D is the diameter (m).

$$\frac{L}{D} = a(m^*)^b \tag{2}$$

where L is the visible flame height (m), D is the diameter (m), a and b are coefficients, and m^* is the dimensionless mass flow.

$$\frac{L}{D} = 0.69(m^*)^{0.41} \tag{3}$$

where L is the visible flame height (m), D is the diameter (m), and m^* is the dimensionless mass flow.

3.3. Axial Temperature. The axial temperature distribution of the jet fire plume of three nozzles with different diameters is shown in Figure 7.

The temperature attenuation law of nozzles with different diameters has good consistency. The flame temperature fluctuation range is roughly between 400 and 1000 °C. The fire plume temperature of a single-diameter nozzle shows a tendency to first rise to the temperature peak and then decay, and its axial spatial distribution conforms to classic three-zone theory. Peak fire plume temperature of the large-diameter nozzle is slightly greater than that of the small-diameter nozzle. In addition, the axial position of the temperature peak of the large-diameter nozzle is higher than the axial position of that of the small-diameter nozzle. This is due to the entrainment formed by the turbulence in the boundary layer and thermal buoyancy. Flame entrainment efficiency of a single-diameter nozzle increases as the flame height increases. Therefore, the oxygen at the bottom of the flame is not enough to support the fuel combustion, and insufficient combustion results in a lower flame temperature. However, there is sufficient oxygen in the middle of the flame to participate in the combustion reaction, which promotes a significant increase in flame temperature. The excess oxygen at the top of the flame cools the flame and causes the flame temperature to drop. The large-diameter nozzle mixes fuel and oxygen more fully, which increases the peak temperature of the fire plume. As the fuel ejection speed of the large-diameter nozzle increases, the fuel cannot take part in the combustion reaction in time. Eventually, the peak position of the fire plume temperature shifts upward.

A transformer oil jet fire plume temperature function relation suitable for nozzles of different diameters was obtained. Based on the prediction expression (4) of the fire plume temperature distribution proposed by Gomez-Mares,[29] the functional formula between the axial centerline temperature and the axial height of the transformer oil jet fire plume is obtained using the experimental data(Figure 8). The experimental data converge to the fitted curve.

https://doi.org/10.1021/acsomega.1c04551
ACS Omega 2021, 6, 31843−31853

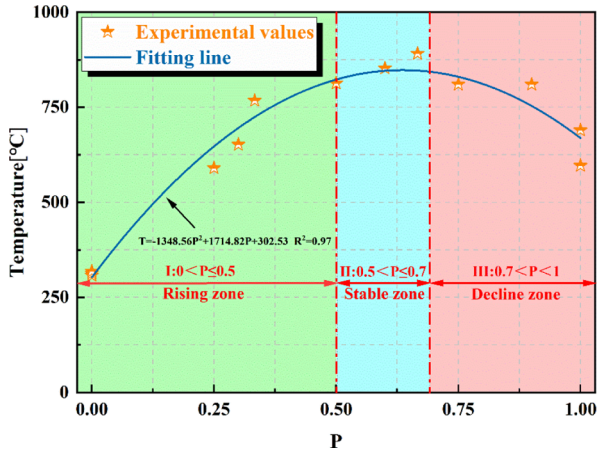

Figure 8. Axial flame plume temperature distribution function.

$$T = a + bp - cp^2 \tag{4}$$

where T is the flame temperature (°C), a, b, and c are coefficients, and p is the percentage of the axial position.

$$p = \frac{z}{L} \tag{5}$$

where L is the visible flame height (m) and z is the distance from the thermocouple location to the bottom of the flame (m).

$$T = -1348.56P^2 + 1714.82P + 302.53 \tag{6}$$

where T is the flame temperature (°C) and p is the percentage of the axial position.

The temperature of the transformer oil jet fire plume can be divided into three areas in the axial space (Figure 8): the growth area ($0 < P < 0.5$), the stable area ($0.5 < P < 0.7$), and the descending area ($0.7 < P < 1$). In this paper, the three regions divided are similar to Gomez's classification results, but there are still some differences. The flame temperature is mainly affected by three factors: oxygen concentration, combustion reaction rate, and carbon black concentration. In the growth zone, the low oxygen concentration and combustion reaction rate result in a lower flame temperature, overall. In addition, the gas−liquid two-phase flow fuel needs to absorb additional energy to be transformed into gas-phase fuel, which makes the combustion reaction rate low. Therefore, the results of the study are larger than the ascending zone of Gomez. In the plateau zone, the fuel is in the gas phase. There is sufficient oxygen. At this time, the concentration of both conforms to the proportion of the chemical reaction, which promotes the temperature to reach the peak in this zone. A large amount of fuel is used in the upper zone, and the combustion reaction rate in the descending zone begins to decrease. In addition, due to the entrainment effect and the carbon black formation process, the flame is cooled by the entrained air and the energy absorbed by the carbon black particles, which eventually cause the temperature in this area to show a downward trend.

3.4Radiation. The radiative fraction is one key parameter to characterize the jet flame combustion dynamics and to calculate the thermal radiant heat emitted from jet fires.[32] On one hand, the study of the radiation fraction provides basic radiation data for the risk assessment of transformer oil jet fires. On the other hand, it can present data support for estimating the safety distance of oil-filled equipment. The radiation fraction is the ratio of the total radiant energy escaping from the flame to the total heat release rate (χ_R).[33]

$$\chi_R = \frac{\dot{Q}_r}{\dot{Q}} \tag{7}$$

where $\dot{Q}$ is the total heat release rate (kW) and $\dot{Q}_r$ is the total radiant energy escaping from the flame (kW).

$$\dot{Q} = \dot{m}_0 \Delta H_c \tag{8}$$

where $\dot{m}_0$ is the mass flow rate (g s^{-1}) and ΔH_c is the fuel combustion heat (MJ kg^{-1}).

$$\dot{Q}_r = \varepsilon \sigma S_F T f^4 \tag{9}$$

where σ is the Stefan−Boltzmann constant, ε is flame emissivity, S_F is the entire flame area (m^2), and T_f is the mean effective radiation temperature(°C).

$$T_f = \frac{3}{4}(T - T_\infty) + T_\infty \tag{10}$$

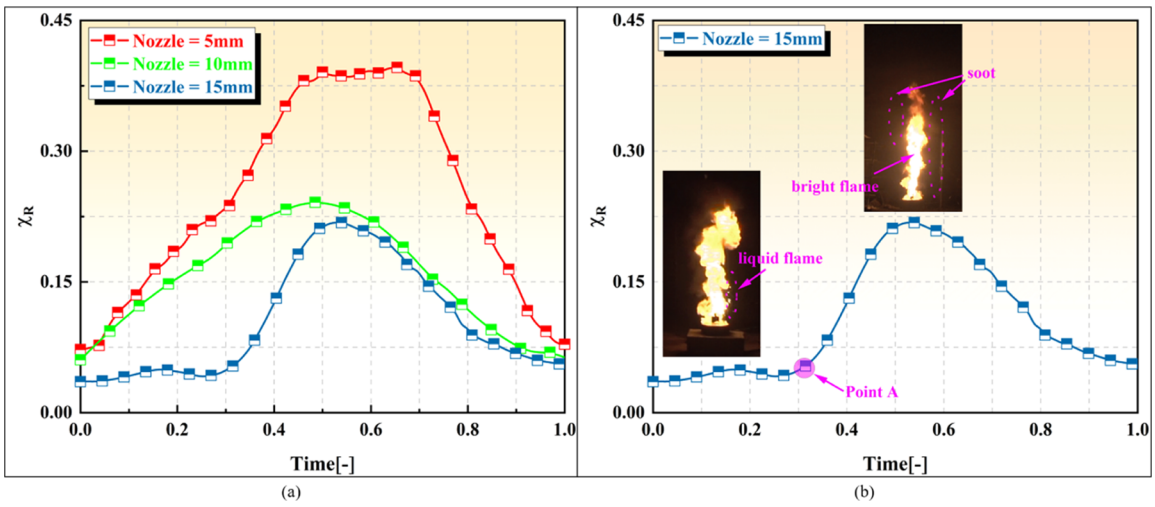

Figure 9. (a) Radiation fraction of three different-diameter nozzles. (b) Radiation fraction and burning pictures for a nozzle diameter of 10 mm.

https://doi.org/10.1021/acsomega.1c04551
ACS Omega 2021, 6, 31843−31853

where T is the flame temperature (°C) and T_∞ is the ambient temperature (°C).

The radiation fraction change curves of the three different-diameter nozzles are shown in Figure 9. The jet fire radiation fraction of nozzles with different diameters has a similar development trend. As the jet fire develops, the radiation fraction increases to a peak and then drops significantly. The peak radiation fraction fluctuates roughly in the range of 0.21−0.39. Obviously, the jet fire radiation fraction of the gas−liquid two-phase flow is higher than the jet fire radiation fraction of the pure gas phase. The radiation fraction decreases as the nozzle diameter increases. In the initial stage of combustion, the radiation fraction of the large-diameter nozzle remained basically stable, and the growth rate of the radiation fraction after point A was significantly higher than that of the small-diameter nozzle. This is because transformer oil is a multi-carbon fuel, and the radiation of the carbon black particle product dominates the jet flame radiation heat flux. Turns[46] proposed the following relationship between the radiation fraction and the residence time of carbon black through research.

$$\chi_R = \frac{\sigma V_f T f^4 \varphi_s}{\dot{Q}} \sim \frac{\sigma V_f T f^4 Y_s}{\dot{Q}} \sim \frac{\sigma V_f T f^4 \tau_f}{\dot{Q}\tau_s} \tag{11}$$

where σ is the Stefan−Boltzmann constant, V_f is the entire flame volume (m^3), φ_s is the carbon black volume fraction (%), T_f is the mean effective radiation temperature (°C), Y_s is the carbon black concentration (%), τ_f is the carbon black residence time (s), τ_s is the carbon black formation time (s), and $\dot{Q}$ is the total heat release rate (kW).

The soot residence time refers to the movement time of soot in the flame. The ejection speed of fuel increases with the increase in the nozzle diameter. The initial particles used to form carbon black particles are affected by the high-speed moving fuel, which reduces the time for the initial particles to transform into carbon black particles through surface growth and aggregation. In addition, with the increase in the combustion reaction rate, the heat release rate of the flame increases significantly, resulting in a decrease in the radiation fraction. At the initial stage of the jet fire combustion of the large-diameter nozzle, the gas−liquid two-phase flow is ejected from the nozzle at a high speed, and the carbon black formation is less, and the radiation fraction remains basically unchanged. The carbon black particles are generated in the carbon black formation zone and move up to the oxidation zone to accumulate. It can be seen that the bright flame is accompanied by a large amount of black smoke, and the radiation fraction increases sharply.

Currently, there are two models for estimating flame radiation heat transfer, namely, the field model and the semi-empirical model. The semi-empirical model is widely used because of its simplicity. The solid flame model predicts that the experimental results of the far field and the near field are in good agreement, so it is often used to evaluate the radiant heat flux of the jet flame to the surrounding environment.[34−39]

$$\dot{q}'' = F_{\vec{1}\to 2} E\tau \tag{12}$$

where I is the calculated radiant heat flux (kW), $F_{1\to 2}$ is the view factor, E is surface emissive power (kW m^{-2}), and τ is atmospheric transmissivity.

$$E = \varepsilon\sigma T f^4 \tag{13}$$

where ε is flame emissivity, σ is the Stefan−Boltzmann constant, and T_f is the mean effective radiation temperature (°C), T_f = 1200.

$$\tau = 0.79\left(\frac{100}{h}\right)^{1/16}\left(\frac{30.5}{x}\right)^{1/16} \tag{14}$$

where h is the ambient relative humidity (%) and x is the radial distance from flame surface (m).

$$F_{\vec{1}\to 2} = F_{A_1\to A_2} = \frac{1}{A_1}\int_{A_2}\int_{A_1}\frac{\cos(\theta_1)\cos(\theta_2)}{\pi R^2}\,dA_1\,dA_2 \tag{15}$$

where A_1 is the area of the flame body (m^2), A_2 is the area of the target (m^2), and R is the linear distance from the surface of the flame body to the target (m).

View factor calculations can be very complicated if the flame shape is not properly chosen. Therefore, it is necessary to determine the shape of the jet fire flame before calculating the view factor. Through experiments and theoretical research, domestic and foreign scholars[15,16,47] have proposed that a cylindrical shape is the most reasonable shape of a vertical jet flame. Therefore, the cylindrical shape is selected as the flame shape to deduce a radiation model. The research method of Beyler[48] is used in the process of deriving the view factor (Figure 10).

$$F_{\vec{1}\to 2} = F_{V_1\to A_2} + F_{V_2\to A_2} \tag{16}$$

$$F_{V_1\to A_2} = \frac{1}{\pi s}\tan^{-1}\left(\frac{h_1}{\sqrt{s^2-1}}\right) - \frac{h_1}{\pi s}\tan^{-1}\sqrt{\frac{s-1}{s+1}} + \frac{A_1 h_1}{\pi s\sqrt{A2^2-1}}\tan^{-1}\sqrt{\frac{(s-1)(A_1+1)}{(s+1)(A_1-1)}} \tag{17}$$

$$F_{V_2\to A_2} = \frac{1}{\pi s}\tan^{-1}\left(\frac{h_2}{\sqrt{s^2-1}}\right) - \frac{h_2}{\pi s}\tan^{-1}\sqrt{\frac{s-1}{s+1}} + \frac{A_2 h_2}{\pi s\sqrt{A2^2-1}}\tan^{-1}\sqrt{\frac{(s-1)(A_2+1)}{(s+1)(A_2-1)}} \tag{18}$$

$$s = \frac{2L}{D} \tag{19}$$

$$h_1 = \frac{2H_1}{D},\ h_2 = \frac{2H_2}{D} \tag{20}$$

$$A_1 = \frac{h1^2 + s^2 + 1}{2s},\ A_2 = \frac{h2^2 + s^2 + 1}{2s} \tag{21}$$

where L is the horizontal distance from the heat flow meter receiving surface to the flame centerline (m), H_1 is the distance between the heat flow meter and the upper boundary of the flame in the vertical direction (m), and H_2 is the distance between the heat flow meter and lower boundary of flame in the vertical direction (m).

The shape and volume of the flame body can determine the optical path length and absorption−emission coefficient. The optical path length and the absorption−emission coefficient together determine the flame emissivity. The flame surface radiation power depends on the flame emissivity and the effective radiation temperature. Therefore, in order to establish

https://doi.org/10.1021/acsomega.1c04551
ACS Omega 2021, 6, 31843−31853

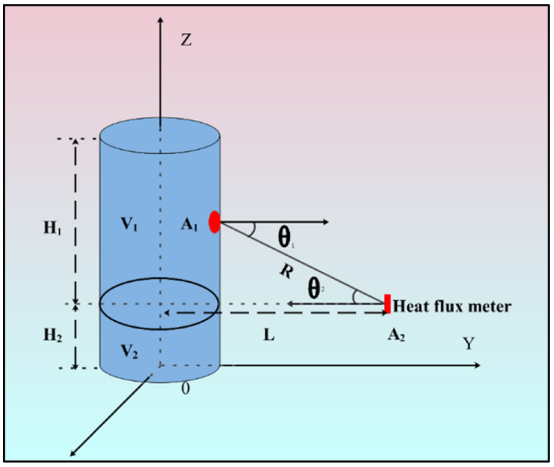

Figure 10. Schematic diagram of view factor calculation.

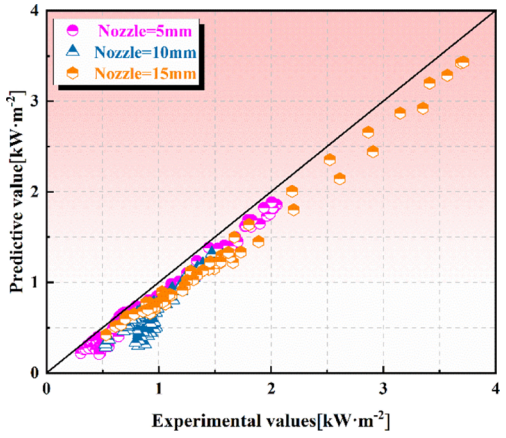

Figure 11. Comparison of the predicted value of the model with the measured value of the experiment.

the radiation power formula of the entire flame surface, the following three hypotheses are proposed:

(i) The flame is idealized as a vertical cylinder emitting thermal radiation from its surface.
(ii) The flame body is an isothermal gray body with a constant absorption−emission coefficient.
(iii) The optical path length of the micro-element surface at a certain height of the flame body is equivalent to the optical path length of the cylinder of the same volume and radius to the side wall surface.

$$\varepsilon = 1 - \exp(-1.8r\kappa) \tag{22}$$

where κ is the extinction coefficient of smoke particles, $\kappa = 3.3$, and r is the flame radius (m).

The combined formula (12−15, 23) obtained the radiant heat flux model of the jet fire flame of the oil-filled equipment in the substation

$$\dot{q}'' = F_{\bar{1}\to 2} \times 5.67 \times 10^{-8} \times 1200^4 \times [1 - \exp(-5.94r)] \tag{23}$$

where r is the flame radius (m) and $F_{1\to 2}$ is the view factor.

Figure 11 shows the experimental values and model predictions of the radiant heat flux of nozzles with different diameters. The predicted value of the model is lower than the experimental value. This may be because the radiant heat flux emitted by the external heat source was measured during the experiment, which was not considered by the model. However, the predicted value and the experimental value still maintain satisfactory consistency. Therefore, the radiation model is of great significance for actual fire prevention and control.

4. CONCLUSIONS

In this paper, a series of transformer oil jet fire combustion experiments with different nozzle diameters are carried out to study the combustion characteristics of transformer oil jet fires in substation oil-filled equipment. During the experiment, the mass loss rate, flame height, axial centerline temperature of the fire plume, and radiant heat flux were measured and analyzed. The main conclusions are as follows:

(i) The jet fire combustion process of oil-filled equipment can be divided into three stages: growth stage, decay stage, and extinction stage. Using the dimensionless flame height and the dimensionless mass flow rate, the correlation between the two is obtained: $L/D = 0.69(m^*)0.41$. The flame height increases with the increase in the mass flow rate.

(ii) The experimental data of axial centerline temperature and axial height of flame plume are fitted to form a functional relationship. Based on the research of Gomez, the functional relationship between the temperature of the axial centerline of the fire plume and the height is obtained: $T = -1348.56P^2 + 1714.82P + 302.53$. The temperature of the transformer oil jet fire plume in the axial space can be divided into three regions, namely, the growth zone ($0 < P < 0.5$), the stable zone ($0.5 < P < 0.7$), and the descending zone ($0.7 < P < 1$).

(iii) It is determined that the peak jet flame radiation fraction fluctuates roughly in the range of 0.39−0.21 under different nozzle diameters. Based on the solid flame model, a prediction model for the jet fire radiant heat flux of the oil-filled equipment in the substation is established: $\dot{q}'' = F_{\bar{1}\to 2} \times 5.67 \times 10^{-8} \times 1200^4 \times [1 - \exp(-5.94r)]$. The predicted value is in good agreement with the experimental value.

This paper changes the nozzle diameter to study the combustion characteristics of the transformer oil jet fire. The research results have important theoretical guiding significance for the prevention and control of jet fires in substations. Based on the consideration of the scale effect, the project team plans to further carry out research on meso-scale and real-scale substation fire experiments to improve the research of the substation jet fire combustion characteristics. The research results will improve the precious data support and theoretical guidance for the actual fire prevention of the substation. Moreover, because the formation mechanism of the jet fire of oil-filled equipment is still unclear, the project team intends to carry out research on the formation mechanism of the oil jet fire of transformers in order to improve the theoretical reference for subsequent research.

AUTHOR INFORMATION

Corresponding Author

Peng Chen − *School of Emergency Management and Safety Engineering and State Key Laboratory of Coal Resources and Safety Mining, China University of Mining and Technology-*

https://doi.org/10.1021/acsomega.1c04551
ACS Omega 2021, 6, 31843−31853

Beijing, Beijing 100083, China; orcid.org/0000-0001-9335-3638; Email: chenpengcumtb@163.com

Authors

Ruibang Sun − *School of Emergency Management and Safety Engineering, China University of Mining and Technology-Beijing, Beijing 100083, China*

Juncai Wang − *School of Emergency Management and Safety Engineering, China University of Mining and Technology-Beijing, Beijing 100083, China*

Xing Yang − *School of Emergency Management and Safety Engineering, China University of Mining and Technology-Beijing, Beijing 100083, China*

Complete contact information is available at: https://pubs.acs.org/10.1021/acsomega.1c04551

Notes

The authors declare no competing financial interest.

■ ACKNOWLEDGMENTS

This work is supported by the Science and Technology project of the State Grid Corporation of China (8000-201918445A-0-0-00).

■ REFERENCES

(1) Cannone, N.; Piccinelli, S. Changes of rock glacier vegetation in 25 years of climate warming in the Italian Alps. *Catena* **2021**, *206*, 105562.

(2) Christina, A. J.; Salam, M. A.; Rahman, Q. M.; Islam, M. A.; Wen, F.; Ang, S. P.; Hasan, S.; Voon, W. Investigation of failure of high voltage bushing at power transformer. *J. Electrost.* **2018**, *96*, 49−56.

(3) Ding, Y.; Mu, C.; Wu, T.; Hu, G.; Zou, D.; Wang, D.; Li, W.; Wu, X. Increasing cryospheric hazards in a warming climate. *Earth-Sci. Rev.* **2021**, *213*, 103500.

(4) Rouabeh, J.; M'Barki, L.; Hammami, A.; Jallouli, I.; Driss, A. Studies of different types of insulating oils and their mixtures as an alternative to mineral oil for cooling power transformers. *Heliyon* **2019**, *5*, No. e01159.

(5) Salama, M. M. M.; Mansour, D.-E. A.; Daghrah, M.; Abdelkasoud, S. M.; Abbas, A. A. Thermal performance of transformers filled with environmentally friendly oils under various loading conditions. *Int. J. Electr. Power Energy Syst.* **2020**, *118*, 105743.

(6) Shi, S.; Liu, G.; Li, Z.; Ye, X. Elevation-dependent growth trends of forests as affected by climate warming in the southeastern Tibetan Plateau. *For. Ecol. Manage.* **2021**, *498*, 119551.

(7) Zeng, J.; Tong, W.; Tang, T. How do energy policies affect industrial green development in China: Renewable energy, energy conservation, or industrial upgrading? *Chinese J. Popul. Resour. Environ.* **2020**, *18*, 79−86.

(8) Zhang, G.; Nan, Z.; Zhao, L.; Liang, Y.; Cheng, G. Qinghai-Tibet Plateau wetting reduces permafrost thermal responses to climate warming. *Earth Planet. Sci. Lett.* **2021**, *562*, 116858.

(9) Zhou, Z.; Chen, G.; Zhou, C.; Hu, K.; Zhang, Q. Experimental study on determination of flame height and lift-off distance of rectangular source fuel jet fires. *Appl. Therm. Eng.* **2019**, *152*, 430−436.

(10) Gómez-Mares, M.; Zárate, L.; Casal, J. Jet fires and the domino effect. *Fire Saf. J.* **2008**, *43*, 583−588.

(11) Imamura, T.; Hamada, S.; Mogi, T.; Wada, Y.; Horiguchi, S.; Miyake, A.; Ogawa, T. Experimental investigation on the thermal properties of hydrogen jet flame and hot currents in the downstream region. *Int. J. Hydrogen Energy* **2008**, *33*, 3426−3435.

(12) Mogi, T.; Shiina, H.; Wada, Y.; Dobashi, R. Experimental study on the hazards of the jet diffusion flame of liquefied dimethyl ether. *Fuel* **2011**, *90*, 2508−2513.

(13) Zhang, Q.-x.; Liang, D.; Wen, J. Experimental study of flashing LNG jet fires following horizontal releases. *J. Loss Prev. Process Ind.* **2019**, *57*, 245−253.

(14) Palacios, A.; Rengel, B. Flame shapes and thermal flux of vertical hydrocarbon flames. *Fuel* **2020**, *276*, 118046.

(15) Palacios, A.; García, W.; Rengel, B. Flame shapes and thermal fluxes for an extensive range of horizontal jet flames. *Fuel* **2020**, *279*, 118328.

(16) Palacios, A.; Casal, J. Assessment of the shape of vertical jet fires. *Fuel* **2011**, *90*, 824−833.

(17) Liu, J.; Zhang, X.; Xie, Q. Flame geometrical characteristics of downward sloping buoyant turbulent jet fires. *Fuel* **2019**, *257*, 116112.

(18) Bradley, D.; Gaskell, P. H.; Gu, X.; Palacios, A. Jet flame heights, lift-off distances, and mean flame surface density for extensive ranges of fuels and flow rates. *Combust. Flame* **2016**, *164*, 400−409.

(19) Laboureur, D. M.; Gopalaswami, N.; Zhang, B.; Liu, Y.; Mannan, M. S. Experimental study on propane jet fire hazards: Assessment of the main geometrical features of horizontal jet flames. *J. Loss Prev. Process Ind.* **2016**, *41*, 355−364.

(20) Gao, Z. H.; Liu, Z. X.; Wan, H. X.; Zhu, J. P. Experimental study on longitudinal and transverse temperature distribution of sidewall confined ceiling jet plume. *Appl. Therm. Eng.* **2016**, *107*, 583−590.

(21) McCaffrey, B. J. Purely Buoyant Diffusion Flames Some Experimental Results National Bureau of Standards. *NBSIR* **1979**, 79−1910.

(22) Hu, L.; Wang, Q.; Tang, F.; Delichatsios, M.; Zhang, X. Axial temperature profile in vertical buoyant turbulent jet fire in a reduced pressure atmosphere. *Fuel* **2013**, *106*, 779−786.

(23) Zukoski, E. E.; Kubota, T.; Cetegen, B. Entrainment in fire plumes. *Fire Saf. J.* **1981**, *3*, 107−121.

(24) Zhang, X.; Hu, L.; Zhu, W.; Zhang, X.; Yang, L. Axial temperature profile in buoyant plume of rectangular source fuel jet fire in normal- and a sub-atmospheric pressure. *Fuel* **2014**, *134*, 455−459.

(25) Tao, C.; Qian, Y.; Tang, F.; Wang, Q. Experimental investigations on temperature profile and air entrainment of buoyancy-controlled jet flame from inclined nozzle bounded the wall. *Appl. Therm. Eng.* **2017**, *111*, 510−515.

(26) Audouin, L.; Kolb, G.; Torero, J. L.; Most, J. M. Average centerline temperatures of a buoyant pool fire obtained by image processing of video recordings. *Fire Saf. J.* **1995**, *24*, 167−187.

(27) Heskestad, G. Virtual Origins of Fire Plumes. *Fire Saf. J.* **1983**, *5*, 109−114.

(28) Wang, Z.; Zhou, K.; Zhang, L.; Nie, X.; Wu, Y.; Jiang, J.; Dederichs, A. S.; He, L. Flame extension area and temperature profile of horizontal jet fire impinging on a vertical plate. *Process Saf. Environ. Prot.* **2021**, *147*, 547−558.

(29) Gómez-Mares, M.; Muñoz, M.; Casal, J. Axial temperature distribution in vertical jet fires. *J. Hazard. Mater.* **2009**, *172*, 54−60.

(30) Zhou, K.; Wang, X.; Liu, M.; Liu, J. A theoretical framework for calculating full-scale jet fires induced by high-pressure hydrogen/natural gas transient leakage. *Int. J. Hydrogen Energy* **2018**, *43*, 22765−22775.

(31) Palacios, A.; Rengel, B. Computational analysis of vertical and horizontal jet fires. *J. Loss Prev. Process Ind.* **2020**, *65*, 104096.

(32) Lowesmith, B. J.; Hankinson, G. Large scale high pressure jet fires involving natural gas and natural gas/hydrogen mixtures. *Process Saf. Environ. Prot.* **2012**, *90*, 108−120.

(33) Zhou, K.; Qin, X.; Wang, Z.; Pan, X.; Jiang, J. Generalization of the radiative fraction correlation for hydrogen and hydrocarbon jet fires in subsonic and chocked flow regimes. *Int. J. Hydrogen Energy* **2018**, *43*, 9870−9876.

(34) Palacios, A.; Muñoz, M.; Darbra, R. M.; Casal, J. Thermal radiation from vertical jet fires. *Fire Saf. J.* **2012**, *51*, 93−101.

(35) Mashhadimoslem, H.; Ghaemi, A.; Palacios, A.; Hossein Behroozi, A. A new method for comparison thermal radiation on large-scale hydrogen and propane jet fires based on experimental and computational studies. *Fuel* **2020**, *282*, 118864.

(36) Schefer, R. W.; Houf, W. G.; Williams, T. C.; Bourne, B.; Colton, J. Characterization of high-pressure, underexpanded hydrogen-jet flames. *Int. J. Hydrogen Energy* **2007**, *32*, 2081−2093.
(37) Hu, L.; Wang, Q.; Delichatsios, M.; Lu, S.; Tang, F. Flame radiation fraction behaviors of sooty buoyant turbulent jet diffusion flames in reduced- and normal atmospheric pressures and a global correlation with Reynolds number. *Fuel* **2014**, *116*, 781−786.
(38) Zhou, K.; Jiang, J. Thermal Radiation From Vertical Turbulent Jet Flame: Line Source Model. *J. Heat Transfer* **2016**, *138*, 042701.
(39) Zhang, B.; Liu, Y.; Laboureur, D.; Mannan, M. S. Experimental Study on Propane Jet Fire Hazards: Thermal Radiation. *Ind. Eng. Chem. Res.* **2015**, *54*, 9251−9256.
(40) Hankinson, G.; Lowesmith, B. J. A consideration of methods of determining the radiative characteristics of jet fires. *Combust. Flame* **2012**, *159*, 1165−1177.
(41) Gómez-Mares, M.; Muñoz, M.; Casal, J. Radiant heat from propane jet fires. *Exp. Therm. Fluid Sci.* **2010**, *34*, 323−329.
(42) Kang, Y.; Wang, Q.; Lu, X.; Ji, X.; Wang, H.; Guo, Q.; Chen, Y.; Yan, J.; Zhou, J. Experimental and theoretical study on radiative heat transfer characteristics of dimethyl ether jet diffusion flame. *Fuel* **2015**, *158*, 684−696.
(43) Zhou, K.; Liu, J.; Jiang, J. Prediction of radiant heat flux from horizontal propane jet fire. *Appl. Therm. Eng.* **2016**, *106*, 634−639.
(44) Otsu, N. A Threshold Selection Method from Gray-level Histograms. *IEEE Trans. Syst. Man Cybern.* **1979**, *9*, 62−66.
(45) Rengel, B.; Àgueda, A.; Pastor, E.; Casal, J.; Planas, E.; Hu, L.; Palacios, A. Experimental and computational analysis of vertical jet fires of methane in normal and sub-atmospheric pressures. *Fuel* **2020**, *265*, 116878.
(46) Turns, S. R.; Myhr, F. H. Oxides of Nitrogen Emissions from Turbulent Jet Flames: Part 1–Fuel Effects and Flame Radiation. *Combust. Flame* **1991**, *87*, 319−335.
(47) Zhou, K.; Wang, Y.; Zhang, L.; Wu, Y.; Nie, X.; Jiang, J. Effect of nozzle exit shape on the geometrical features of horizontal turbulent jet flame. *Fuel* **2020**, *260*, 116356.
(48) Beyler, C. L. Fire Hazard Calculations for Large, Open Hydrocarbon Fires. In *SFPE Handbook of Fire Protection Engineering*, 2016; pp 2591−2663.

https://doi.org/10.1021/acsomega.1c04551
ACS Omega 2021, 6, 31843−31853